Acta Crystallographica Section D
Biological Crystallography
ISSN 0907-4449

Peculiarity in crystal packing of anti-HIV lectin actinohivin in complex with α(1–2)mannobiose

Kaoru Suzuki,[a] Masaru Tsunoda,[b] M. Mominul Hoque,[b,c] Fang Zhang,[d] Jiandong Jiang,[d] Xiaoxue Zhang,[d] Naomi Ohbayashi,[b] Haruo Tanaka[b,d,e] and Akio Takénaka[b,d,f]*‡

[a]College of Science and Engineering, Iwaki Meisei University, Iwaki, Fukushima 970-8551, Japan, [b]Faculty of Pharmacy, Iwaki Meisei University, Iwaki, Fukushima 970-8551, Japan, [c]Department of Biochemistry and Molecular Biology, Rajshahi University, Rajshahi, Bangladesh, [d]Graduate School of Science and Engineering, Iwaki Meisei University, Iwaki, Fukushima 970-8551, Japan, [e]KIIM Pharm. Lab. Inc., Fukushima 970-8551, Japan, and [f]Graduate School of Bioscience and Biotechnology, Tokyo Institute of Technology, Yokohama 226-8501, Japan

‡ Present address: Research Institute, Chiba Institute of Technology, Narashino, Chiba 275-0016, Japan.

Correspondence e-mail: atakenak@sakura.email.ne.jp

Received 22 February 2013
Accepted 28 June 2013

PDB References: actinohivin–α(1–2)mannobiose complex, 4end; 4g1r

Previously, the anti-HIV lectin actinohivin (AH) was cocrystallized with the target α(1–2)mannobiose (MB) in the apparent space group $P2_13$. However, three MB-bound AH rotamers generated by ±120° rotations around the molecular pseudo-threefold rotation axis are packed randomly in the unit cell according to $P2_12_12_1$ symmetry [Hoque *et al.* (2012). *Acta Cryst.* D**68**, 1671–1679]. It was found that the AH used for crystallization contains short peptides attached to the N-terminus [Suzuki *et al.* (2012). *Acta Cryst.* F**68**, 1060–1063], which cause packing disorder. In the present study, the fully mature homogeneous AH has been cocrystallized with MB into two new crystal forms at different pH. X-ray analyses of the two forms reveal that they have peculiar character in that the space groups are the same, $P22_12_1$, and the unit-cell parameters are almost the same with the exception of the length of the *a* axis, which is doubled in one form. The use of homogeneous AH resulted in the absence of disorder in both crystals and an improvement in the resolution, thereby establishing the basis for AH binding to the target MB. In addition, the two crystal structures clarify the interaction modes between AH molecules, which is important knowledge for understanding the multiple binding effect generated when two AH molecules are linked together with a short peptide [Takahashi *et al.* (2011). *J. Antibiot.* **64**, 551–557].

1. Introduction

Actinohivin (AH) is a potent anti-HIV lectin of actinomycete origin that blocks HIV entry into susceptible cells (Chiba *et al.*, 2001, 2004). AH contains 114 amino acids and consists of three segments, each of which has a carbohydrate-binding site. AH has no or very low affinity to glycoproteins carrying only one high-mannose-type glycan (HMTG) such as RNase B, but exhibits a strong and specific affinity to glycoproteins having many HMTGs such as the HIV surface protein gp120 (Tanaka *et al.*, 2009). In addition, AH does not possess cytotoxicity, mitogenic activity and chemokine/cytokine-inducible activity (Hoorelbeke *et al.*, 2010; Matoba *et al.*, 2010). Thus, AH is an excellent candidate for development as an antiretroviral drug to treat or prevent HIV infection.

In order to obtain structural insights into the anti-HIV activity of AH, we solved the crystal structures of unbound AH (Tanaka *et al.*, 2009) and its complex with the target D1 chain α(1–2)mannobiose (MB) moiety of HMTG attached to HIV-1 gp120 (Hoque *et al.*, 2012). The latter study showed that the three AH rotamers generated by ±120° rotation around the molecular pseudorotation axis are packed randomly in the unit cell according to the $P2_12_12_1$ symmetry and that the whole crystal exhibits an apparent space group $P2_13$ as an averaged structure (Hoque *et al.*, 2012). The $P2_12_12_1$ space group can be

Table 1
Crystallization conditions, statistics of data collection and structure determination, and crystallographic data.

Values in parentheses are for the highest resolution shell.

Crystal (PDB code)	AH-MB-2 (4end†)	AH-MB-3 (4g1r†)
Crystallization condition‡		
Sample solution (in pure water)		
AH (mg ml^{-1})	10	10
MB (mg ml^{-1})	20	20
Reservoir solution		
$(NH_4)_2SO_4$ (*M*)	2.0	—
$NH_4H_2PO_4$ (*M*)	—	0.2
Tris–HCl pH 8.5 (*M*)	—	0.1
Precipitant	5% PEG 400	50% MPD
pH (mixed solution)	4.4	6.2
Temperature (K)	298	298
Data collection		
X-ray source	PF BL-5A	PF BL-5A
Wavelength (Å)	1.00	1.00
Detector	ADSC Quantum 210r	ADSC Quantum 210r
Resolution (Å)	27.84–1.90 (1.95–1.90)	12.45–1.57 (1.65–1.57)
Crystal system	Orthorhombic	Orthorhombic
Unique reflections	10409 (696)	33286 (3996)
Completeness (%)	99.9 (100)	95.4 (80.2)
R_{merge}§	0.111 (0.348)	0.061 (0.076)
$R_{p.i.m.}$§	0.068 (0.158)	0.026 (0.048)
Multiplicity	6.5 (6.6)	6.1 (3.1)
$\langle I/\sigma(I)\rangle$	11.2 (4.6)	20.8 (10.4)
Crystal data		
Space group	$P22_12_1$	$P22_12_1$
Unit-cell parameters (Å)		
a	27.8	54.8
b	67.1	66.9
c	66.8	66.9
Z¶	1	2
V_M (Å^3 Da^{-1})	2.49	2.44
Structure determination		
R factor	0.164 (0.209)	0.160 (0.163)
R_{free}††	0.231 (0.275)	0.194 (0.172)
Protein atoms	886	1772
Water atoms	144	276
MB atoms	69	138
Acetonitrile atoms	6	—
R.m.s.d., bonds (Å)	0.022	0.023
R.m.s.d., angles (°)	1.91	2.12

† The origins of the atomic coordinates differ between the two crystals in the eight crystallographical equivalents. ‡ The droplet consisted of sample and reservoir solutions in an equal volume ratio. § See Evans (2006) for definitions. ¶ Number of single proteins in the asymmetric unit. †† For 5% of the observed data (Brünger, 1992).

raised to $P2_13$ by adding a threefold symmetry along the body-diagonal direction. It is rare that an asymmetric macromolecule crystallizes according to the crystallographic symmetry based on its pseudomolecular symmetry. The structure analysis of AH in complex with MB (AH-MB-1) gave a definite structure since the molecular symmetry was high enough to give a high resolution of 1.60 Å. However, some parts were still ambiguous owing to packing disorder and further efforts to obtain non-disordered crystals failed. The reason for the failure was that the AH samples prepared were heterogeneous, *i.e.* they contain N-terminal extension fragments from the linker region between the signal peptide and the mature AH. The length of the extension fragments depends on the duration of cultivation of the AH-producing strain (Suzuki *et al.*, 2012). We succeeded in obtaining the mature AH with high homogeneity from a 20 d culture. The

Table 2
Intensity statistics along with $I/N\sigma$.

Average intensity of AH-MB-3: $\langle I(h = 2n + 1)\rangle = 7433.5$, $\langle I(h = 2n)\rangle = 51726.5$. $R_{ug}(I) = \langle I(h = 2n + 1)\rangle/\langle I(h = 2n)\rangle = 0.144$. $R_{st}(I) = \sum_h |I_2(h) - I_3(h/2)|/(1/2)\sum_h I_2(h) + I_3(h/2) = 0.238$, where I_2 and I_3 are the intensity data for for the AH-MB-2 and AH-MB-3 crystals, respectively.

	No. of reflections		
$I/N\sigma$	AH-MB-2	AH-MB-3 ($h = 2n + 1$)	AH-MB-3 ($h = 2n$)
$0 \le N < 1$	239	546	196
$1 \le N < 2$	356	1057	410
$2 \le N < 3$	391	1300	519
$3 \le N < 4$	425	1392	603
$4 \le N < 5$	398	1433	733
$5 \le N < 6$	365	1366	861
$6 \le N < 7$	356	1267	890
$7 \le N < 8$	335	1156	914
$8 \le N < 9$	292	1131	874
$9 \le N < 10$	258	1119	849
$10 \le N < 11$	256	1240	791
$11 \le N < 12$	223	1327	910
$12 \le N < 13$	194	1353	1000
$13 \le N < 14$	208	1194	1410
$14 \le N < 15$	194	879	1556
$15 \le N < 16$	167	534	1651
$16 \le N < 17$	174	213	1971
$17 \le N < 18$	146	78	1706
$18 \le N < 19$	163	58	595
$19 \le N < 20$	162	45	143
$20 \le N$	3253	376	918

AH sample thus obtained was successfully crystallized with high reproducibility in two different crystal forms from the $P2_13$ crystal of AH-MB-1 (Suzuki *et al.*, 2012). The new crystals (AH-MB-2 and AH-MB-3) appeared under acidic and slightly acidic (near-neutral) conditions without potassium ions. They belong to the same space group $P22_12_1$ and diffracted well, but were different from each other in that the length of the *a* axis of the unit cell of AH-MB-3 is twice that of AH-MB-2. These facts are also an additional peculiarity in the crystallography of AH. The two crystal structures have been determined at 1.9 and 1.57 Å resolution, respectively. This paper will describe the details of their structural features including molecular interactions.

2. Materials and methods

The preparation and crystallization of fully matured AH have already been reported in the previous paper (Suzuki *et al.*, 2012). Two different crystals (AH-MB-2 and AH-MB-3) were obtained under the conditions listed in Table 1. The crystals were mounted on Cryo-Loops (Hampton Research) for flash-cooling. X-ray experiments were performed at 100 K using synchrotron radiation of wavelength 1.00 Å on beamline BL-5A at the Photon Factory (Tsukuba, Ibaraki, Japan). Diffraction images were recorded on an ADSC Quantum 210r CCD detector (Area Detector Systems). A total of 180 frames for each crystal were taken at 1° oscillation steps with 1 s exposure per frame. The raw data images were indexed and the intensities around Bragg spots were integrated, scaled and merged using *MOSFLM* and *SCALA* (Battye *et al.*, 2011) from the *CCP*4 suite (Winn *et al.*, 2011). The intensities were converted to structure-factor amplitudes with *TRUNCATE*

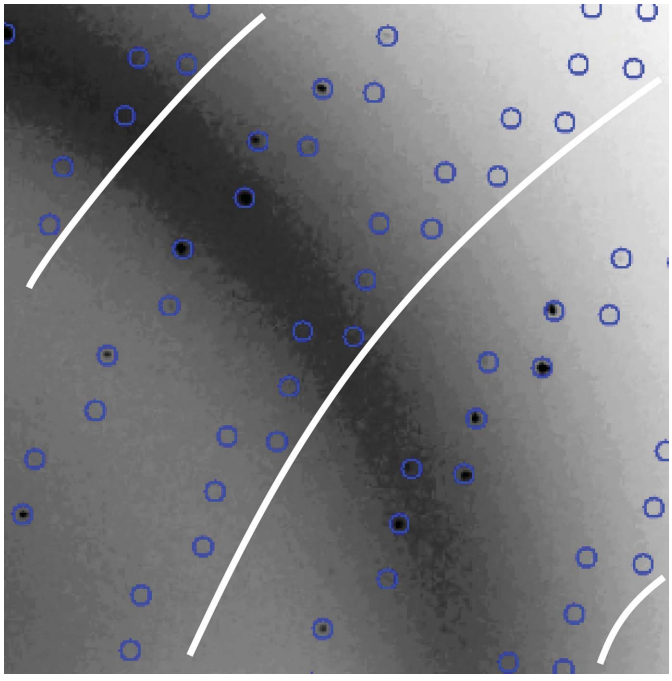

Figure 1
A diffraction pattern of the AH-MB-2 crystal. Circles indicate possible positions of Bragg reflections predicted for a hypothetical unit cell with twice the *a*-axis length (2 × 27.8 Å), after indexing using the program *HKL-2000*. The spots at $h = 2n$ have significant intensities, while those at $h = 2n + 1$ near the white lines have no significant intensities.

(French & Wilson, 1978) from the *CCP*4 suite. The crystallographic data are listed in Table 1, together with data-collection statistics.

The approximate phase angles of the reflections were estimated by the molecular-replacement technique in the program *AMoRe* (Navaza, 1994) from *CCP*4 with the unbound form of AH (PDB entry 3a07; Tanaka *et al.*, 2009) as a phasing probe. The replaced AH atomic parameters were refined by the restrained maximum-likelihood least-squares technique using *REFMAC*5 (Murshudov *et al.*, 2011) from *CCP*4. The bound MB, acetonitrile and water molecules were assigned to peaks in $F_o - F_c$ maps. After several steps of *REFMAC* refinements with these additional atoms, the molecular structures were revised by interpreting OMIT maps at every residue using the program *Coot* (Emsley & Cowtan, 2004). The stereochemistry of the protein structures was verified using the program *PROCHECK* (Laskowski *et al.*, 1993). Statistical data of the structure determination are summarized in Table 1.

3. Results and discussion

3.1. Crystallographic peculiarity

AH-MB-2 and AH-MB-3 crystals were obtained under acidic (pH 4.4) and slightly acidic (pH 6.2) conditions, respectively. As shown in Table 1, they belonged to the same space group $P22_12_1$ and diffracted well to 1.9 Å (AH-MB-2) and 1.57 Å (AH-MB-3) resolution. The lengths of the *b* and *c* axes are similar but the two crystals never showed tetragonal symmetry in their diffraction-intensity distributions. The striking difference between the two crystals is that the length of the *a* axis of AH-MB-3 is equal to almost twice that of AH-MB-2. The lattice constants of AH-MB-2 suggest that AH molecules with dimensions 27 × 33 × 33 Å are packed in the unit cell in the form of a flat square box. We speculated that the two crystals are composed of layers, with AH-MB-2 having identical layers stacked on each other and AH-MB-3 having two types of layers stacked alternately. In order to determine whether this speculation is warranted, we calculated the values of $R_{ug}(I)$ and $R_{st}(I)$ defined by the following equations:

$$R_{ug}(I) = \langle I(h = 2n + 1)\rangle / \langle I(h = 2n)\rangle \quad (1)$$

and

$$R_{st}(I) = \sum_h |I_2(h) - I_3(h/2)| / (1/2) \sum_h I_2(h) + I_3(h/2), \quad (2)$$

where n is an integer. $R_{ug}(I)$ is the ratio of the averaged intensities of reflections with h even to those of reflections with h odd. A low $R_{ug}(I)$ value indicates that the layers are similar and a value of zero indicates that the layers are identical. $R_{st}(I)$ is the overall difference between the intensity data of AH-MB-2 and AH-MB-3; the extent of the difference (or similarity) between the layers may be inferred from its value. In addition to these parameters, Table 2 shows some characteristic differences in the intensity distributions between the two data sets.

The $R_{ug}(I)$ value of AH-MB-3 data is remarkably low at 0.144. However, the distribution of $I(h = 2n + 1)/\sigma$ along σ shows that the odd reflections have significant intensities. To compare the diffraction patterns of the two crystals, the diffraction patterns of the AH-MB-2 crystal were indexed using the same unit-cell parameters except for the length of the *a* axis, which was doubled. Fig. 1 shows an example of the indexed patterns. The intensities of the Bragg spots at $h = 2n$ are significant, while those at $h = 2n + 1$, marked with circles, are insignificant. This feature is observed in all of the diffraction patterns of the AH-MB-2 crystal. These results thus confirm that the two crystals are substantially different.

To calculate the $R_{st}(I)$ value, the two data sets of AH-MB-2 and AH-MB-3 were scaled by a least-squares method using the corresponding reflections when h of AH-MB-2 is doubled. The $R_{st}(I)$ value is also low at 0.238 when the intensity data $I(h = n)$ of AH-MB-2 are compared with $I(h = 2n)$ of AH-MB-3. This is slightly higher than the *R*-factor values of the refined structures. An extremely low $R_{st}(I)$ value means that the layers are very similar. We therefore conclude that the AH-MB-3 crystal is composed of two layers of AH molecules similar to each other but not the same and that they are shifted at half of the *a*-axis length along the *a* axis.

3.2. Nondisordered structure of AH in complex with MB

In the previous paper, we reported that the crystal of the complex between AH and MB exhibits an apparent space group $P2_13$ as an averaged structure and that the MB-bound AH molecules are disordered in the $P2_12_12_1$ unit cell with the molecular pseudo-threefold symmetry. Although the two new

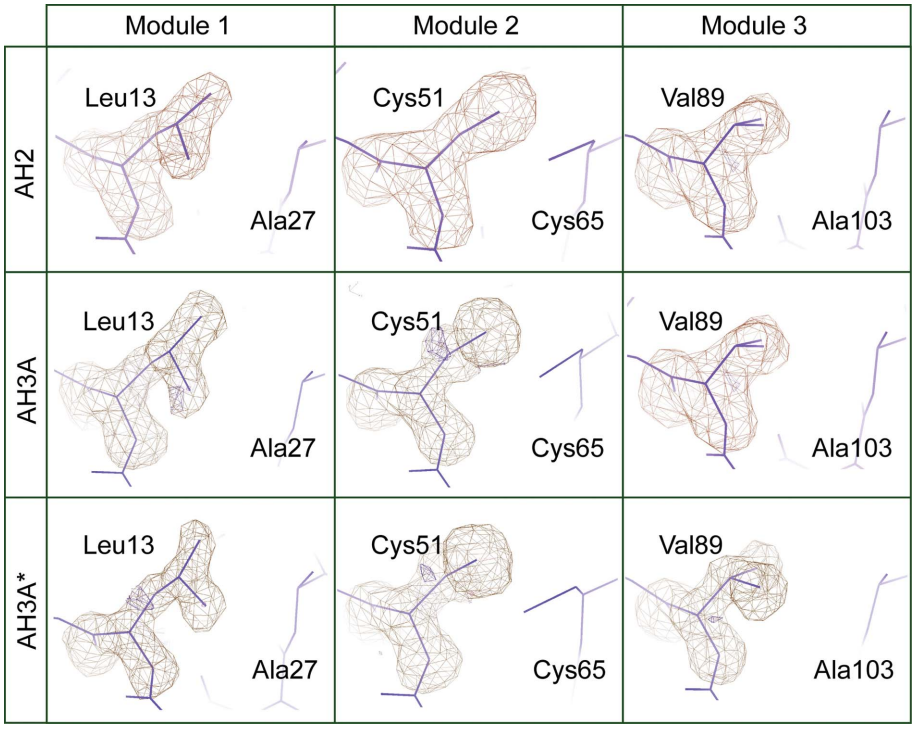

Figure 2
OMIT maps of Leu13 in module 1, Cys51 in module 2 and Val89 in module 3 of the AH molecules (contoured at the 3.0σ level). AH2, AH3A and AH3A* indicate the AH molecules found in the AH-MB-2 crystal and the two molecules, A and A*, found in the AH-MB-3 crystal, respectively. In the molecules, the three residues that were omitted from the density calculations fit well into the densities. This indicates that the AH molecules are not disordered in both crystals.

crystal structures were fully refined to reasonable *R*-factor and $R_{\rm free}$ values (Table 1), we were interested in examining the existence of disorder similar to that observed in the previous structure. OMIT maps were calculated without the Leu13, Cys51 and Val89 residues, which are exposed to Ala27, Cys65 and Ala103, respectively. These residues are disordered in the $P2_13$ unit cell by the pseudo-threefold symmetry. We hypothesized that if the AH molecules are disordered like they are in the $P2_13$ form (Hoque *et al.*, 2012) then the three residues would exhibit a similar electron-density distribution. However, as shown in Fig. 2, the three residues have distinct density shapes and fit well into their respective densities in both AH-MB-2 and AH-MB-3, verifying the absence of packing disorder.

3.3. Crystal packing of MB-bound AH molecules

Fig. 3 shows the packing diagrams of the two crystals. As mentioned above, in the AH-MB-2 crystal the MB-bound AH molecules are packed in the unit cell in the form of a flat square box as expected from the space-group symmetry of the crystal. The AH molecules form a layered structure (A) perpendicular to the *a* axis, with the A layers being stacked along the *a* axis (hereafter referred to as the A–A stack). In the AH-MB-3 crystal, the two MB-bound AH molecules form two different layers (A and A*) and the two layers are stacked alternately along the *a* axis (hereafter referred to as the A–A* stack).

Fig. 4 shows the interaction geometries of adjacent molecules. Within a molecular layer of A or A*, hydrogen-bond interactions are found between AH molecules related by the crystallographic twofold symmetry in the central region marked 1 in Fig. 3(*a*). A direct hydrogen bond that links the hydroxyl group of Tyr94 and the peptide carbonyl O atom of Thr10 occurs in the two independent layers of the AH-MB-3 crystal. However, in the AH-MB-2 crystal the hydroxyl group of Tyr94 is indirectly hydrogen bonded *via* a bridging water molecule to the peptide carbonyl O atom of Thr10. In the two other regions marked 2 and 3 (Fig. 4*b*), three MB-bound AH molecules (labelled *B*, *C* and *D* and related by the crystallographic symmetry) form a cluster through direct hydrogen bonds, such that an AH molecule comes in contact with the first mannose residues (Man^1) of MB bound to the adjacent AH molecules. These inter actions are commonly found in both crystals.

As shown in Fig. 3(*b*), the two layers A and A* of AH-MB-3 appear to be stacked along the *a* axis, but they are in fact slightly displaced. This is the reason why the average intensity of reflections with *h* odd is remarkably low in the AH-MB-3 data. Figs. 3(*c*) and 3(*d*) show a few differences in the layer interactions between the A–A and A–A* stacks, which occur in the four regions marked with broken lines. As shown in Fig. 4(*c*), the direct hydrogen-bond interactions in the A–A* stack occur between the peptide NH of the Ser2 residue in layer A and the carbamoyl O atom of Asn19 extruding from layer A* and between the carboxyl O atom of the C-terminal Gly114 residue in layer A and the carbamoyl N atom of Asn21 in layer A*. These interactions are also found in the A–A stack of the AH-MB2 crystal. The interactions that are only found in the AH-MB-3 crystal (Fig. 4*d*) are that between the peptide NH of Ser77 in layer A and the carboxyl O atom of Asp57 in layer A* and that between the side-chain hydroxyl group of Ser77 in layer A and the carbonyl O atom of Asp57 in layer A*. It is noteworthy that in place of these interactions in the AH-MB-2 crystal (Fig. 4*e*), Asp57, the carboxyl group of which changes its conformation around the $C^{\alpha}-C^{\beta}$ bond, forms hydrogen bonds to water molecules. In other words, one of the major differences between AH-MB-2 and AH-MB-3 is that in the latter Asp57 participates in direct interaction between two layers. This difference might be attributed to the crystallization conditions, which may influence whether Asp57 adopts the dissociated or neutral form.

3.4. Overall structure of AH and MB

As shown in Fig. 5, a total of three MB-bound AH structures have been found in the present study: an AH molecule (AH2) in the AH-MB-2 crystal and two AH molecules (AH3A and AH3A*) in the AH-MB-3 crystal. They appear to be quite similar to each other, to that found in the AH-MB-1 crystal (Hoque *et al.*, 2012) and to unbound AH (Tanaka *et al.*, 2009). Each AH molecule is composed of the three modules generated from the three tandem repeats in the amino-acid sequence. All module structures in the MB-bound states are virtually identical, with an average r.m.s. deviation of 0.45 Å between C^{α} atoms (Table 3). In the unbound forms, the two additional N-terminal residues are definitely visible in the electron-density map. In the AH-MB-1 crystal, however, it was difficult to assign these N-terminal residues, even in the final $F_o - F_c$ map, owing perhaps to the packing disorder of the whole molecule. Fully matured homogeneous AH molecules were used for crystallization in the present study and the AH molecules in the new crystals are not disordered, with the two N-terminal residues assigned without ambiguity and their atomic parameters fully refined. The N-terminal Ser2 and the C-terminal Gly114 residues are both involved in the interactions between the two layer structures of AHs described above.

In each AH molecule, three MB molecules are bound in the three modules. Their conformations are similar to each other, as shown in Fig. 6, and to those found in AH-MB-1 (Hoque *et al.*, 2012). The two mannose residues (Man^1 and Man^2) are linked by the α(1–2) bond and form a compact bracket-shaped conformation through two C—H···O interactions [average C···O distances of 3.05 Å between $C^1(Man^2)$ and $O(Man^1)$ and of 3.48 Å between $C^5(Man^1)$ and $O(Man^2)$].

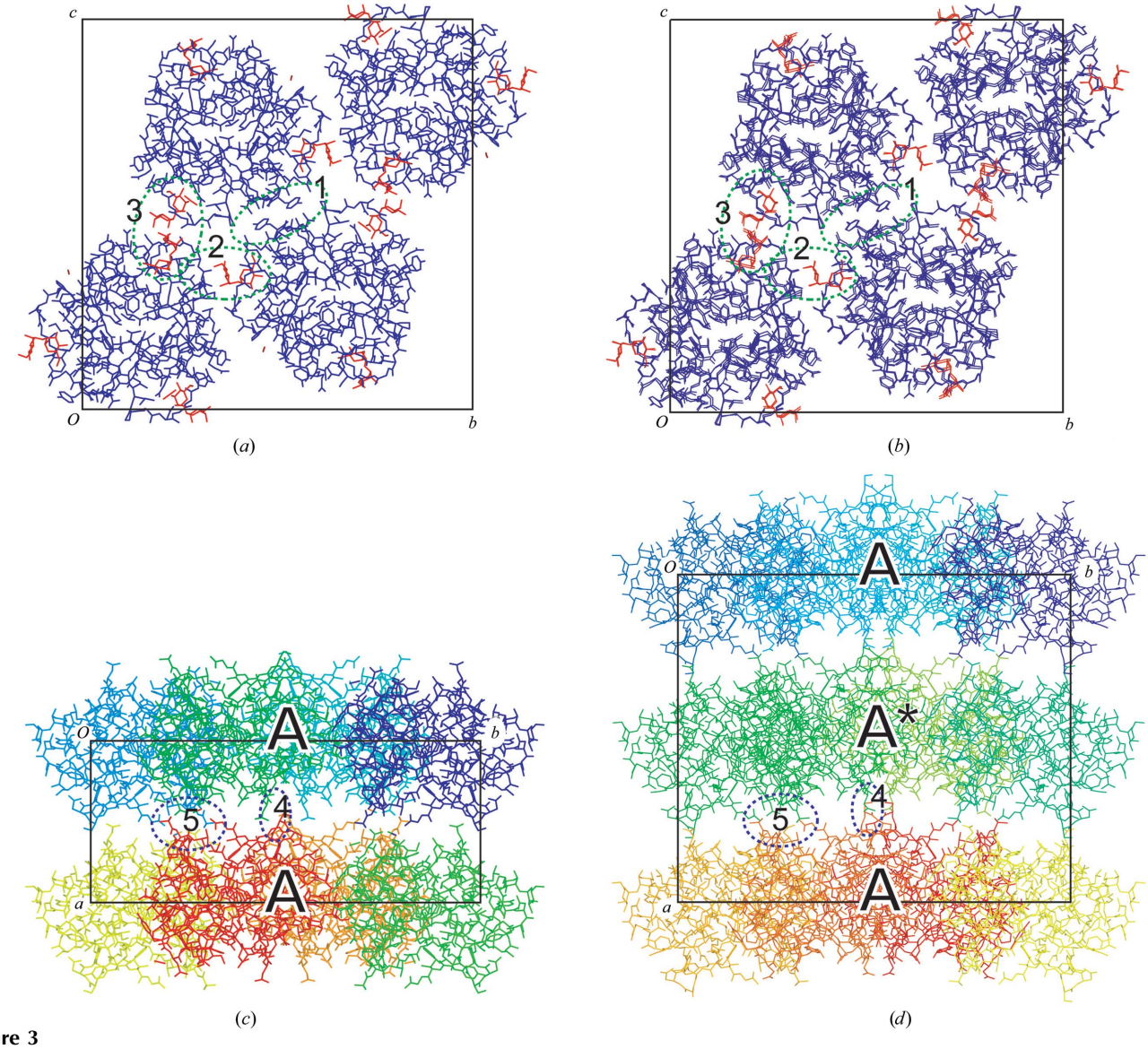

Figure 3
Packing diagrams of the AH molecules in the AH-MB-2 (left column) and AH-MB-3 (right column) crystals, viewed down the *a* axis (*a*, *b*) and down the *c* axis (*c*, *d*). Circles with broken lines indicate regions in which AH molecules directly interact with each other in the lateral direction within a layer and between the two layers stacked along the *a* axis (or the A–A and A–A* stacks).

3.5. Binding geometry of AH with the target mannobiose

The three modules of AH are structurally equivalent and such equivalence may support the high pseudo-symmetry of the molecule. As shown in Fig. 6, the three β-strands form a convex slope on the lateral surface and a long loop runs to form the rim of a shallow pocket in each module. The rim is occupied by the first mannose residue (Man^1) of MB, which is exposed to the solvent region. The pocket accommodates the second mannose residue (Man^2), the C^3, C^4 and C^5 atoms of which are secured in the pocket by four hydrogen bonds to AH residues. Specifically, the Asp91 residue of AH forms two hydrogen bonds to Man^2, in which one of the two carboxyl O atoms accepts the hydroxyl group attached to the C^3 atom of Man^2 (average O$\cdots$O distance of 2.6 Å) and another O atom accepts the hydroxyl group at the C^4 atom of the same Man^2 (average O$\cdots$O distance of 2.6 Å). In addition, the O^3 and O^4 atoms of Man^2 accept the carbamoyl amide N atom of Asn104 (average N$\cdots$O distance of 2.9 Å) and the hydroxyl group of Tyr99 (average O$\cdots$O distance of 2.7 Å), respectively. This MB recognition mode is conserved in other modules and in the AH molecules found in other AH-MB crystals. These structural features are consistent with mutational data on AH indicating the importance of these residues for target binding (Takahashi *et al.*, 2010). The side chain of Tyr108 is wedged between and forms hydrophobic contacts with the two Man residues. The methyl group of Leu101 appears to lock the C^3 atom of Man^2 in position, such that the hydroxyl group attached to the C^1 atom in the axial configuration protrudes into the outside in an upwards direction. It would be interesting to clarify the roles played by Tyr108 and Leu101 in MB recognition through mutational experiments.

The target HMTG is composed of the three mannobiose branches (D1, D2 and D3). D1 is preferentially bound to AH and is thus the major binding branch, whereas D3 is only weakly bound to AH or the minor binding branch (Hoque *et*

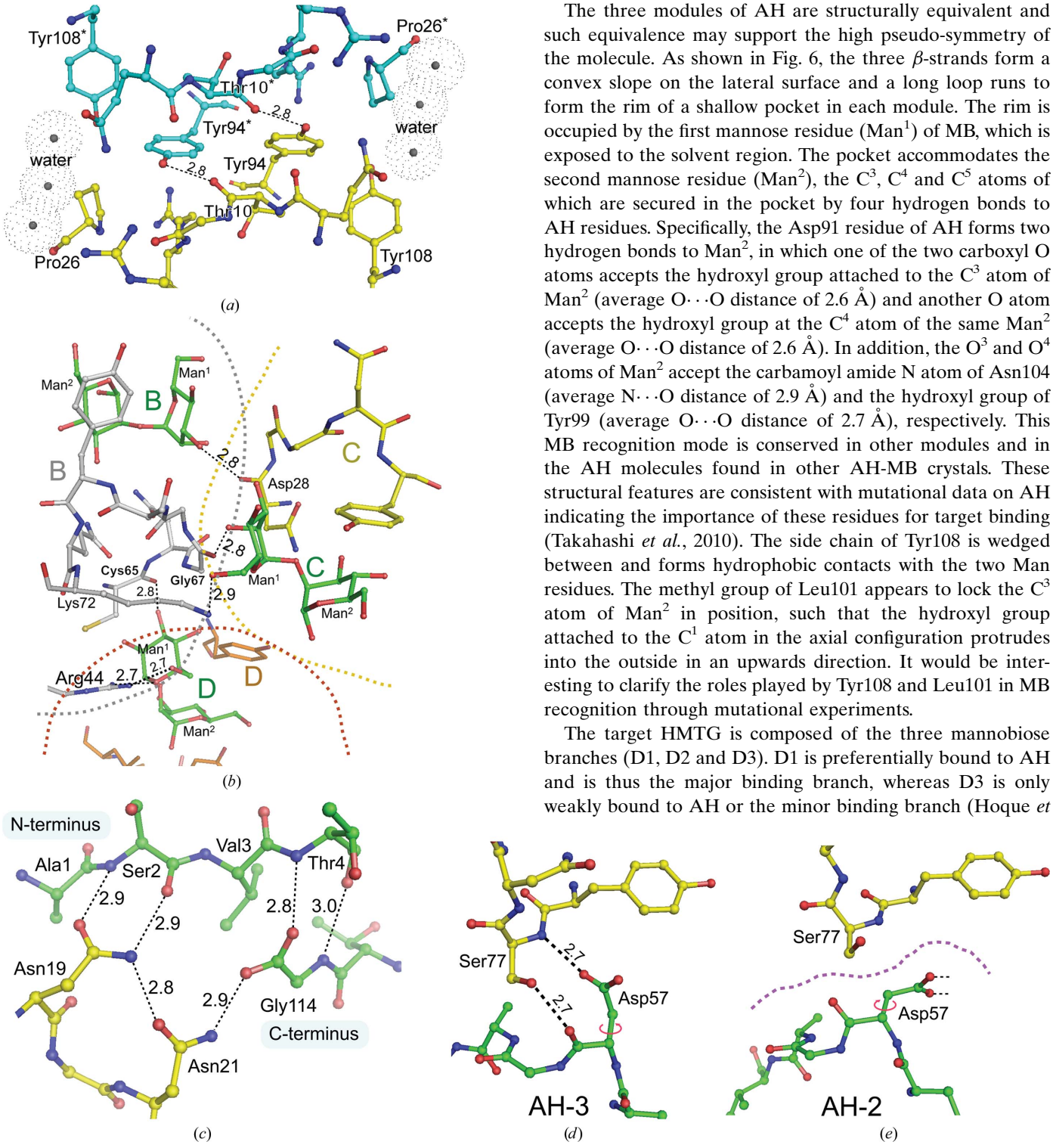

Figure 4
Molecular interaction geometry. Within a molecular layer, the AH molecules related by the crystallographic twofold symmetry in the central region marked 1 in Fig. 3(*a*) are linked by direct hydrogen bonds (*a*). These interactions can be found in both layers of the AH-MB-3 crystal. However, the interactions are not direct (water-mediated) in the corresponding locations in the AH-MB-2 crystal. In the regions marked 2 and 3, there are six direct hydrogen-bond interactions (*b*) which form a cluster composed of three AH molecules. These interactions occur between the Man^1 residues and the neighbouring AH molecules. Between two layers, there are two types of direct contacts of AHs: those bridging the N-terminal and C-terminal residues from one layer and two Asn residues from an adjacent layer (*c*) and those linking the Asp57 residue of one layer and the Ser77 residue of an adjacent layer (*d*). The former type is found in both crystals, while the latter is only found in the AH-MB-3 crystal. In the AH-MB-2 crystal, the side-chain conformation of Asp57 changes to interact with water molecules (*e*).

Table 3
R.m.s. deviations (Å) of corresponding atoms in the two superimposed structures.

In the case of proteins, only the C^{α} atoms are superimposed. AH1 and AH2 are the AH molecules found in the AH-MB-1 and AH-MB-2 crystals, respectively, while AH3A and AH3A* are the two AH molecules found in the AH-MB-3 crystal. MB1, MB2 and MB3 are bound in modules 1, 2 and 3, respectively.

(*a*) AH3A.

AH1	0.37
AH2	0.32
AH3A*	0.15

(*b*) MB1(AH3A).

MB1(AH1)	0.44
MB2(AH1)	0.33
MB3(AH1)	0.31
MB1(AH2)	0.33
MB2(AH2)	0.35
MB3(AH2)	0.37
MB2(AH3A)	0.37
MB3(AH3A)	0.34
MB1(AH3A*)	0.33
MB2(AH3A*)	0.32
MB3(AH3A*)	0.34

al., 2012; Tanaka *et al.*, 2009). The MB-binding pockets in the present AH and MB complex structures are the major binding sites for the MB parts of the D1 branches. As in the case of AH-MB-1, an open space is found between two neighbouring pockets in the present structures, in which Asn/Asp residues are closely localized (Asn17, Asn19 and Asn21 in the first space, Asn55, Asp57 and Ala59 in the second space, and Asn93, Asn95 and Asn97 in the third space). These residues were found to be responsible for AH binding to HMGT (Takahashi *et al.*, 2010). The open space is likely to accept the end of the D3 chain of HMTG (Hoque *et al.*, 2012), which would form hydrophilic interactions with the Asn/Asp residues.

3.6. Structural evidence for the high specificity of AH towards the target mannobiose

The present study confirmed that the three MB-binding pockets of AH are almost the same or equivalent and that their tertiary structures are rather rigid. Likewise, the bracket-shaped conformation of MB also appears to be rigid. The rigidity of the structures helps to ensure that only the target mannobiose may bind to AH. In addition, the presence of three binding pockets in an AH would mean that one AH molecule could simultaneously bind three HMTGs of gp120. This binding feature is quite different from those proposed for other lectins, cyanovirin-N (CV-N; Botos *et al.*, 2002) and greffithsin (Ziółkowska *et al.*, 2007; Moulaei *et al.*, 2010), and may bring about its high specificity for HMTGs. As described

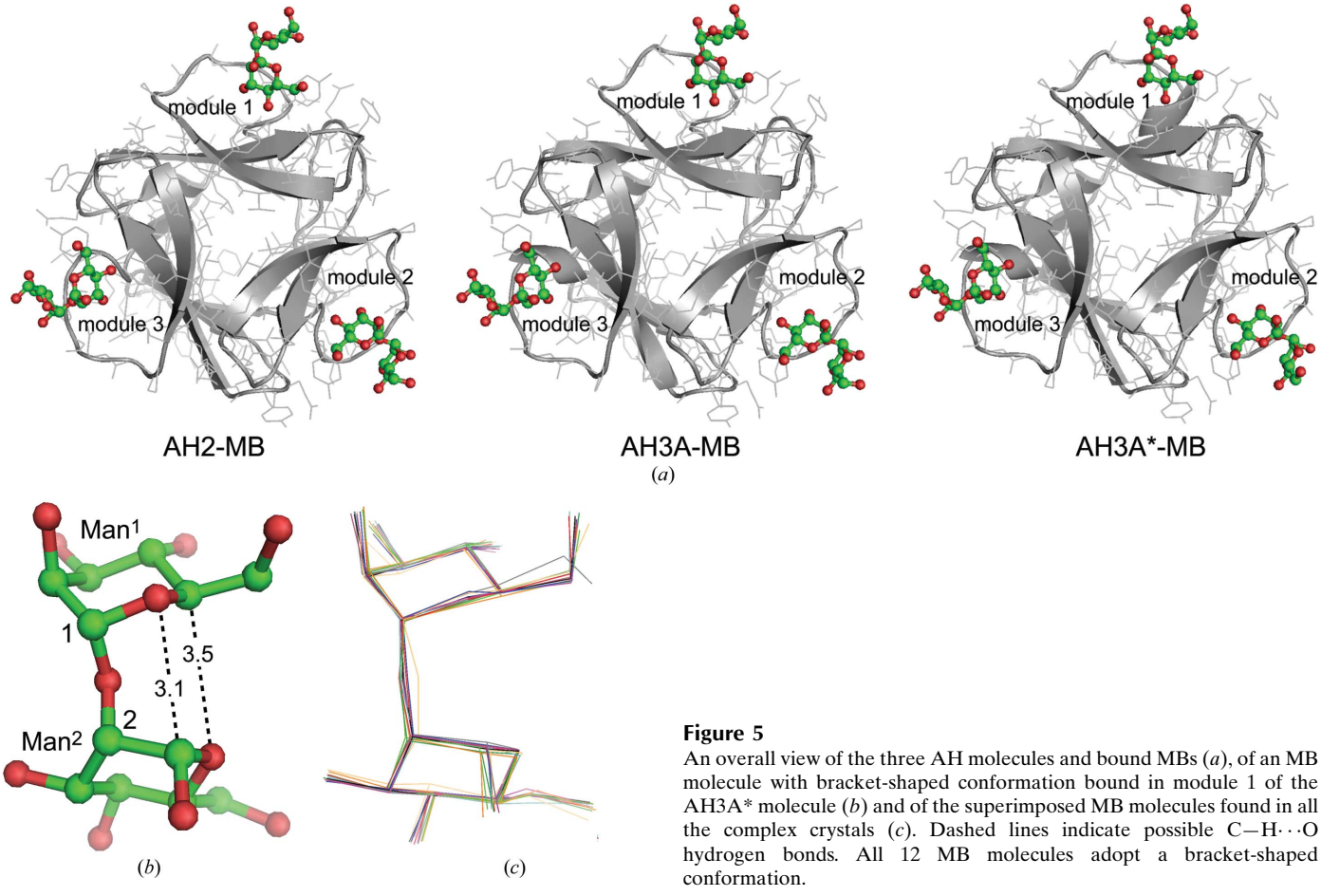

Figure 5
An overall view of the three AH molecules and bound MBs (*a*), of an MB molecule with bracket-shaped conformation bound in module 1 of the AH3A* molecule (*b*) and of the superimposed MB molecules found in all the complex crystals (*c*). Dashed lines indicate possible C—H···O hydrogen bonds. All 12 MB molecules adopt a bracket-shaped conformation.

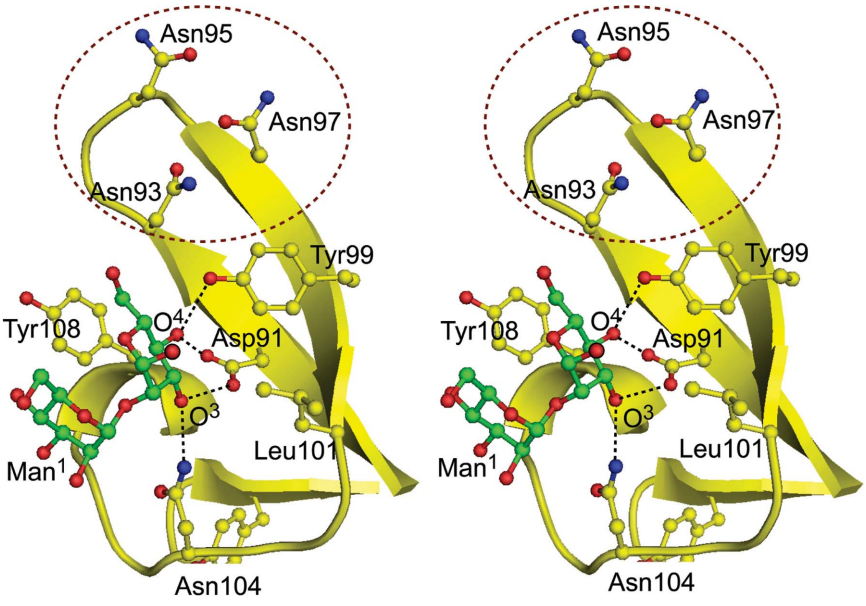

Figure 6
A stereo diagram of MB bound in a pocket of the third module in the AH3A* molecule, in which three Asn residues (enclosed in brown circles) are closely localized. The hydroxyl groups in the equatorial configuration of the Man^2 residue of MB are recognized by four hydrogen bonds (dashed lines). To distinguish the protruding O^1 atom of Man^2 from the rest of the O atoms, it is drawn with a red sphere outlined by a black circle.

previously, the three equivalent binding pockets of AH exhibit the multivalent effect by bridging between HMTGs protruding densely from one side of the HIV-gp120 surface (Hoque *et al.*, 2012; Tanaka *et al.*, 2009). The multivalent effect is further magnified by linking two AH molecules (Takahashi *et al.*, 2011). These facts suggest the necessity of a contribution from the specific AH–AH interaction and collaboration. Those found in the present X-ray structures (Fig. 4) would be useful knowledge not only for understanding the specificity of AH against HIV-1 but also for designing more effective antiretroviral drugs to suppress the infectious expansion of HIV/AIDS and help expedite an end to the HIV/AIDS pandemic in the near future. To ensure this, we are trying to crystallize AH in complex with gp120.

We thank L. Chavas, Y. Yamada, N. Matsugaki, N. Igarashi and S. Wakatsuki (Photon Factory, Tsukuba, Japan) for their assistance in data collection at the synchrotron facility and E. C. Morishita for revising the manuscript. This work was supported in part by grants from the Grants-in-Aid for Scientific Research, the Ministry of Education, Culture, Sports, Science and Technology of Japan (KS and AT), the Tokyo Biochemical Research Foundation (AT), the JAXA-GCF project (MT), the Science Research Promotion Fund, the Promotion and Mutual Aid Corporation for Private Schools of Japan (HT), the Japan Ministry of Health, Labour and Welfare Research and the Japan Health Science Foundation on Drug Innovation (HT). Figs. 1, 2 and 3 were produced with the programs *Coot*/*DINO* (Philippsen, 2003) and *RASMOL* (Sayle & Milner-White, 1995), respectively. Figs. 4, 5 and 6 were produced using *PyMOL* (DeLano, 2002).

References

Battye, T. G. G., Kontogiannis, L., Johnson, O., Powell, H. R. & Leslie, A. G. W. (2011). *Acta Cryst.* D**67**, 271–281.
Botos, I., O'Keefe, B. R., Shenoy, S. R., Cartner, L. K., Ratner, D. M., Seeberger, P. H., Boyd, M. R. & Wlodawer, A. (2002). *J. Biol. Chem.* **277**, 34336–34342.
Brünger, A. T. (1992). *Nature (London)*, **355**, 472–475.
Chiba, H., Inokoshi, J., Nakashima, H., Omura, S. & Tanaka, H. (2004). *Biochem. Biophys. Res. Commun.* **316**, 203–210.
Chiba, H., Inokoshi, J., Okamoto, M., Asanuma, S., Matsuzaki, K., Iwama, M., Mizumoto, K., Tanaka, H., Oheda, M., Fujita, K., Nakashima, H., Shinose, M., Takahashi, Y. & Omura, S. (2001). *Biochem. Biophys. Res. Commun.* **282**, 595–601.
DeLano, W. L. (2002). *PyMOL*. http://www.pymol.org.
Emsley, P. & Cowtan, K. (2004). *Acta Cryst.* D**60**, 2126–2132.
Evans, P. (2006). *Acta Cryst.* D**62**, 72–82.
French, G. S. & Wilson, K. S. (1978). *Acta Cryst.* A**34**, 517–525.
Hoorelbeke, B., Huskens, D., Férir, G., François, K. O., Takahashi, A., Van Laethem, K., Schols, D., Tanaka, H. & Balzarini, J. (2010). *Antimicrob. Agents Chemother.* **54**, 3287–3301.
Hoque, M. M., Suzuki, K., Tsunoda, M., Jiang, J., Zhang, F., Takahashi, A., Ohbayashi, N., Zhang, X., Tanaka, H., Ōmura, S. & Takénaka, A. (2012). *Acta Cryst.* D**68**, 1671–1679.
Laskowski, R. A., MacArthur, M. W., Moss, D. S. & Thornton, J. M. (1993). *J. Appl. Cryst.* **26**, 283–291.
Matoba, N., Husk, A. S., Barnett, B. W., Pickel, M. M., Arntzen, C. J., Montefiori, D. C., Takahashi, A., Tanno, K., Omura, S., Cao, H., Mooney, J. P., Hanson, C. V. & Tanaka, H. (2010). *PLoS One*, **5**, e11143.
Moulaei, T., Shenoy, S. R., Giomarelli, B., Thomas, C., McMahon, J. B., Dauter, Z., O'Keefe, B. R. & Wlodawer, A. (2010). *Structure*, **18**, 1104–1115.
Murshudov, G. N., Skubák, P., Lebedev, A. A., Pannu, N. S., Steiner, R. A., Nicholls, R. A., Winn, M. D., Long, F. & Vagin, A. A. (2011). *Acta Cryst.* D**67**, 355–367.
Navaza, J. (1994). *Acta Cryst.* A**50**, 157–163.
Philippsen, A. (2003). *DINO*. http://www.dino3d.org.
Sayle, R. A. & Milner-White, E. J. (1995). *Trends Biochem. Sci.* **20**, 374.
Suzuki, K., Ohbayashi, N., Jiang, J., Zhang, X., Hoque, M. M., Tsunoda, M., Murayama, K., Tanaka, H. & Takénaka, A. (2012). *Acta Cryst.* F**68**, 1060–1063.
Takahashi, A., Inokoshi, J., Hachiya, A., Oka, S., Omura, S. & Tanaka, H. (2011). *J. Antibiot.* **64**, 551–557.
Takahashi, A., Inokoshi, J., Tsunoda, M., Suzuki, K., Takenaka, A., Sekiguchi, T., Omura, S. & Tanaka, H. (2010). *J. Antibiot.* **63**, 661–665.
Tanaka, H., Chiba, H., Inokoshi, J., Kuno, A., Sugai, T., Takahashi, A., Ito, Y., Tsunoda, M., Suzuki, K., Takénaka, A., Sekiguchi, T., Umeyama, H., Hirabayashi, J. & Omura, S. (2009). *Proc. Natl Acad. Sci. USA*, **106**, 15633–15638.
Winn, M. D. *et al.* (2011). *Acta Cryst.* D**67**, 235–242.
Ziółkowska, N. E., Shenoy, S. R., O'Keefe, B. R., McMahon, J. B., Palmer, K. E., Dwek, R. A., Wormald, M. R. & Wlodawer, A. (2007). *Proteins*, **67**, 661–670.